SCIENCE CHINA
Chemistry

• REVIEWS • Progress of Projects Supported by NSFC
• SPECIAL ISSUE • Chemical Methodology

January 2014 Vol.57 No.1: 70–77
doi: 10.1007/s11426-013-5007-5

# Linear-scaling computation of excited states in time-domain

YAM ChiYung[1,2*] & CHEN GuanHua[1]

[1]*Department of Chemistry, The University of Hong Kong, Pokfulam Road, Hong Kong, China*
[2]*Beijing Computational Science Research Center, Beijing 100084, China*

Received July 13, 2013; accepted August 25, 2013; published online October 24, 2013

The applicability of quantum mechanical methods is severely limited by their poor scaling. To circumvent the problem, linear-scaling methods for quantum mechanical calculations had been developed. The physical basis of linear-scaling methods is the locality in quantum mechanics where the properties or observables of a system are weakly influenced by factors spatially far apart. Besides the substantial efforts spent on devising linear-scaling methods for ground state, there is also a growing interest in the development of linear-scaling methods for excited states. This review gives an overview of linear-scaling approaches for excited states solved in real time-domain.

**linear-scaling methods, quantum chemistry, time-domain, density matrix**

## 1 Introduction

With the dawn of quantum mechanics, its accurate description of microscopic systems allows studies of processes and properties in different materials to be done via simulations on computers without doing experiments. In quantum chemistry, the major goal is to obtain solutions to the atomic or molecular Schrödinger equation. However, in practice, the exact solution of the Schrödinger equation is intractable. Whereas viable approximations have been made, ab initio molecular orbital calculations are usually limited to small- and medium-size molecular systems. The obstacle lies in the rapid increase of computational cost when the systems get large. This poor algorithmic scaling of many existing quantum mechanical methods hinders their applications to large complex systems.

A large number of linear-scaling computational methods are proposed for the ground state calculations [1, 2], allowing simulations of large complex systems that are previously out of reach. Physical properties like optical absorption spectrum, nonlinear polarizabilities, dielectric constant and magnetic properties, however, cannot be accessed through ground state calculations. In addition, studies of chemical reactions require correct description of excited states. To obtain these properties, one has to resort to methods for excited states. In general, the computational demand of excited state calculations is substantially larger than ground state calculations. Despite of the increasing interest in excited state properties, relatively few linear-scaling methods have been developed for the excited states.

There have been many computational methods developed for description of excited states. The present quantum mechanical methods for excited state properties fall into two categories: time-independent and time-dependent approaches. The time-independent approaches solve the stationary Schrödinger equation:

$$\hat{H}\left|\Psi_{\mathrm{k}}\right\rangle = E_{\mathrm{k}}\left|\Psi_{\mathrm{k}}\right\rangle$$

where $\hat{H}$ is the Hamiltonian operator, and $\left|\Psi_{\mathrm{k}}\right\rangle$ is the many-body wavefunction. The eigenvalues $E_{\mathrm{k}}$ and corresponding eigenvectors $\left|\Psi_{\mathrm{k}}\right\rangle$ are the energies and wavefunctions of different electronic states. By solving the time-independent Schrödinger equation, one can obtain

*Corresponding author (email: yamcy@yangtze.hku.hk)

ground state and excited states of interest and this requires the explicit construction of excited states wavefunctions. Excitation energies, for instance, can be obtained from the difference of the energies of these states. On the other hand, the time-dependent approaches start with the electronic ground state wavefunction $|\Psi_0\rangle$ and follow its time evolution after switching on the time-dependent external excitation. The time evolution of the wavefunction can be obtained by solving the time-dependent Schrödinger equation:

$$i\hbar\frac{\partial}{\partial t}|\Psi(t)\rangle = \left[\hat{H}+\hat{V}(t)\right]|\Psi(t)\rangle$$

where $\hat{V}(t)$ is the time-dependent external perturbation. The excited state properties such as optical spectra can then be extracted from the temporal trajectory of the wavefunction. The advantage of this is that one temporal trajectory contains all frequency information which can be obtained by Fourier transformation. Alternatively, the excited state properties can also be obtained through a linear response treatment in frequency-domain, based on the time-dependent perturbation theory. The key quantity here is the linear response function which contains all the information of the excited states.

Within exact treatment, time-independent approaches and time-dependent approaches are equivalent and yield same results. It is, however, usually not the case when approximations are introduced. In general, time-independent methods are more computational demanding since explicit construction of wavefunction for each excited state is required. In time-independent picture, there are existing works devising linear-scaling methods, for instance, Møller-Plesset perturbation theory [3, 4], coupled cluster method [5−7], configuration interaction [8]. They, however, have been applied to ground states only. Instead, linear-scaling methods for excited states have been developed within the time-dependent framework, both in time-domain [9, 10] and frequency-domain [11−17]. In general, the linear-scaling time-domain methods are found to be more efficient while the iterative approaches in linear-scaling frequency-domain methods suffer convergence problem in resonant response [10]. It is noted that a recent frequency-domain method achieves linear-scaling with small prefactor by building localized molecular orbitals (LMOs) from subsystems [17]. As those linear-scaling methods for ground state, the physical basis of linear-scaling methods for excited states is the nearsightedness of density matrices [18]. They are based on the locality in quantum mechanics, which means that the properties of an object are influenced only by its immediate surroundings. Most linear-scaling algorithms are built around the reduced single-electron density matrix or its representation in terms of Wannier functions and take advantage of its decay properties. To achieve linear-scaling, the exponentially decay quantities can be neglected when they are smaller than some threshold value. Kohn [18] proposed "the principle of the nearsightedness of equilibrium systems" to justify the locality of ground-state density matrix. Chen and Mukamel [19] realized that the locality of density matrices persists for many excited states as well, and they showed that the off-diagonal matrix elements are negligible when the distance between the two orbitals is larger than some preset critical lengths.

In this paper, we give an overview of linear-scaling methods for excited states solved in time-domain. Linear-scaling time-domain methods involve solving the Liouville-von Neumann equation, the localized density matrix (LDM) method [10] or the time-dependent Kohn-Sham (TDKS) equation using the non-orthogonal localized molecular orbitals (NOLMOs) [20]. Similar to linear-scaling ground state methods, the major computational bottleneck lies in the construction of Fock matrix and density matrices (or wavefunctions). We review here the numerical techniques to achieve linear-scaling computational time. Applications are given to demonstrate the effectiveness of the linear-scaling time-domain methods.

## 2 Construction of Fock matrix

To reflect the response to the change in electron density, Fock matrix is reconstructed in each time step when the electron density is updated. This involves the Coulomb part and exchange-correlation part. The Coulomb part gives the classical interaction between electron pairs and scales formally as $O(N^4)$. The Coulomb potential is given by:

$$V(\boldsymbol{r}) = \int \frac{\rho(\boldsymbol{r}')}{|\boldsymbol{r}-\boldsymbol{r}'|}\mathrm{d}\boldsymbol{r}' \tag{1}$$

Fast multipole method (FMM) [21, 22] is developed in the 1980's to accelerate the calculation of long-ranged forces between classical point charges. It is later generalized to evaluate the Coulomb potential in the basis of Gaussian-type basis functions [23, 24]. Through multipole expansion, it allows one to group sources that lie close together and treat them as a single source. The method was first applied to the field of computational electromagnetics. The idea was then borrowed and implemented to efficiently treat the Coulomb interaction in Hartree Fock (HF) and density functional theory (DFT) calculations.

For excited state calculations, the Coulomb part contribution to the Fock matrix is given as follows:

$$\int \mathrm{d}\boldsymbol{r}\int \mathrm{d}\boldsymbol{r}'\chi_i(\boldsymbol{r})\chi_j(\boldsymbol{r})\frac{1}{\boldsymbol{r}-\boldsymbol{r}'}\rho(\boldsymbol{r}',t) \tag{2}$$

here $\chi$ are the basis functions, and $\rho$ is the time-dependent electron density constructed from the single-electron density matrix $P(t)$,

$$\rho(\boldsymbol{r},t) = \sum_{ij}\chi_i(\boldsymbol{r})\chi_j(\boldsymbol{r})P_{ij}(t) \tag{3}$$

In the FMM, the whole space is divided into boxes and the different charge distributions are assigned to the corresponding boxes. Each box is further divided into half along each Cartesian axis until the charge distributions in each box at the lowest level are approximately constant, resulting in a hierarchy of boxes. Based on the distance between the boxes, the Coulomb potential is split into near-field and far-field contributions. For near-field potential, explicit analytical integration is used. For far-field contribution, the Coulomb potential is represented by the multipole expansion as follows:

$$V(\boldsymbol{r}) = \frac{Z}{R} + \frac{\mu_\alpha R_\alpha}{R^3} + \frac{Q_{\alpha\beta} R_\alpha R_\beta}{R^5} + \frac{O_{\alpha\beta\gamma} R_\alpha R_\beta R_\gamma}{R^7} + \cdots \quad (4)$$

where $Z$, $\mu$, $Q$ and $O$ are, respectively, the monopole, dipole, quadrupole and octupole. $R$ is the distance from the center of the box. The multipole expansion of the potential stems from charge distributions at higher level boxes can be constructed from their child boxes, resulting in a multipole expansion for each box representing all the charge distributions contained in it. Depending on the distance of the interaction, the multipole expansions from different levels are converted into local Taylor expansions and the expansion coefficients are summed. Since the number of boxes in each level is constant, the Coulomb part of the Fock matrix can be evaluated with linear-scaling efforts.

In general, the near-field evaluation constitutes a dominant part in the computational effort. There are various methods to reduce the computational cost. Different recursive relations [25] had been introduced to speedup the evaluations of two-electron integrals. The J-engine method [26] sums the density matrix directly during the evaluation of two-electron integrals, thus avoiding explicit construction of the full set of two-electron integral intermediates. Resolution of identity (RI) methods [27] speedup the calculations by fitting the electron density with a set of auxiliary basis functions. This approach is further accelerated by combining with the multipole methods, the multipole accelerated RI-J (MARI-J) method [28].

The formation of the Fock matrix involves also the exchange and correlation (XC) terms. Employing the local basis functions, evaluation of the XC potential, $\upsilon^{\mathrm{XC}}$ and its derivatives scales naturally linear with system size. Due to the nature of the XC potential, the integral

$$\langle i | \upsilon^{\mathrm{XC}} | j \rangle = \int \mathrm{d}\boldsymbol{r} \chi_i(\boldsymbol{r}) \upsilon^{\mathrm{XC}}(\boldsymbol{r}) \chi_j(\boldsymbol{r}) \quad (5)$$

cannot be solved analytically and one has to resort to numerical quadrature [29],

$$\langle i | \upsilon^{\mathrm{XC}} | j \rangle \approx \sum_A^N \sum_i^{N_{\mathrm{grid}}^A} p_A w_i \chi_i(\boldsymbol{r}) \upsilon^{\mathrm{XC}}(\boldsymbol{r}) \chi_j(\boldsymbol{r}) \quad (6)$$

where $p_A$ is the nuclear partition function and $w_i$ is the weights of grid point $i$. Due to the local nature of the basis functions, only a constant number of basis function pairs contribute for each grid point in Eq. (6). Efficient screening techniques [30] are developed and linear-scaling behavior is readily achieved.

For HF and hybrid DFT methods, there is also a contribution from the so-called exact exchange. Although the contributions of exact exchange to the Fock matrix arise from the same set of integrals, the FMM cannot be applied to the exchange terms because the FMM requires the contraction of charge distributions with the density matrix from the beginning. However, linear-scaling can be achieved by exploiting the decay of the density matrix with distance. Exact exchange thus involves only a finite number of significant terms and several methods have been developed which exploit the locality of the density matrix to reach a linear-scaling behavior for the exact exchange evaluation [31–33].

## 3 The LDM method

The time-domain LDM method [9] is the first linear-scaling method for excited states, developed in 1998 at semi-empirical level. It was later implemented with time-dependent density-functional theory (TDDFT) [34, 35] and time-dependent density-functional tight-binding method (TDDFTB) [36]. The LDM method has been applied widely to simulate the optical processes of a variety of complex molecular systems such as light harvesting systems [37], carbon nanotubes (CNTs) [38], polymer aggregates [39], water clusters [36] and silicon quantum dots [40].

### 3.1 Formulation

The LDM method solves the Liouville-von Neumann equation:

$$i\hbar \frac{\partial}{\partial t} P(t) = \left[ F(t), P(t) \right] \quad (7)$$

which is equivalent to the time-dependent Schrödinger equation. Here $F(t)$ is the time-dependent Fock matrix and $P(t)$ is the reduced single-electron density matrix. Eq.(7) gives the equation of motion (EOM) for propagation of the density matrix in real time. Starting from Eq. (7), $P(t)$ can be partitioned into two parts,

$$P(t) = P^{(0)} + \delta P(t) \quad (8)$$

where $P^{(0)}$ is the single-electron density matrix representing the ground state in the absence of the external perturbation, and $\delta P(t)$ is the difference between $P(t)$ and $P^{(0)}$. The Fock matrix in Eq. (7) can be divided into three parts,

$$F(t) = F^{(0)} + \delta F(t) + f(t) \quad (9)$$

where $F^{(0)}$ is the ground state Fock matrix and $\delta F(t)$ gives the induced Fock matrix due to the change in electron density, and $f(t)$ represents the interaction between an electron and the external field $\xi(t)$. In atomic orbital (AO) representation,

$$f_{ij}(t) = -\xi(t) \cdot \langle \chi_i | \hat{\boldsymbol{r}} | \chi_j \rangle \tag{10}$$

Eq. (7) can be rewritten as:

$$\begin{aligned} & i\hbar\delta\dot{P} - ([F^{(0)}, \delta P] + [\delta F, P^{(0)}]) \\ & = [f, P^{(0)}] + [\delta F + f, \delta P] \end{aligned} \tag{11}$$

For the first-order induced density matrix $\delta P^{(1)}$, the second term on RHS is eliminated and its dynamics can be described by the following equation:

$$i\hbar\delta\dot{P}^{(1)} - [F^{(0)}, \delta P] + [\delta F, P^{(0)}] = [f, P^{(0)}] \tag{12}$$

More specifically, Eq. (12) can be written as:

$$\begin{aligned} i\hbar\delta\dot{P}_{ij}^{(1)} = & \sum_k \left( F_{ik}^{(0)} \delta P_{kj}^{(1)} - \delta P_{ik}^{(1)} F_{kj}^{(0)} \right) \\ & + \sum_k \left( \delta F_{ik}^{(1)} P_{kj}^{(0)} - P_{ik}^{(0)} \delta F_{kj}^{(1)} \right) \\ & + \sum_k \left( f_{ik} P_{kj}^{(0)} - P_{ik}^{(0)} f_{kj} \right) \end{aligned} \tag{13}$$

Solving Eq. (13) alone does not lead to the linear-scaling of computational time, because the matrix multiplication involved is intrinsically scales as $O(N^3)$. The key for the linear-scaling lies in the reduction of the dimension of the reduced single-electron density matrix which is based on the fact that the density matrix has a localized character. This locality holds not only for the $P^{(0)}$ but also for $\delta P^{(1)}$. Specifically, $P_{ij}^{(0)}$ is set to zero for $r_{ij} > l_0$, where $r_{ij}$ is the distance between the matrix elements $i$ and $j$. Consequently, $F_{ij}^{(0)}$ becomes zero for the same $r_{ij}$; and $\delta P_{ij}^{(1)}$ is set to zero when $r_{ij} > l_1$, here $l_0$ and $l_1$ are cutoff lengths. For a fixed pair of $i$ and $j$, the summations over $k$ in Eq. (13) is finite and independent of system size. This leads to linear-scaling computation of the first and third terms on the RHS of Eq. (13). The second term on the RHS involves also the update of Fock matrix where the numerical algorithms introduced in Section 2 are used to evaluate this term with linear-scaling efforts.

Alternately, a threshold criterion can be used to take the advantage of matrix sparsity, i.e. a matrix element can be safely neglected when it is below a certain threshold value. Asymptotically the number of significant elements in the matrices grows linearly with the system size. Eq. (13) involves only matrix multiplications and additions, and these matrix manipulations can thus be carried out with linear-scaling effort. A standard way is to represent the matrices in a compressed sparse row (CSR) or modified compressed sparse row (MSR) format [41]. The matrix multiplication is then simply carried out by multiplying one pair of matrix elements at a time. Matrix additions or subtractions are straightforward and are far less expensive than multiplications.

Whereas different electronic structure methods have different Fock matrices, the EOM of density matrix (Eq. (7)) remains the same. The LDM method has been implemented with semi-empirical TDHF, first-principles TDDFT and TDDFTB Hamiltonians. Semi-empirical models, such as PPP, INDO, and MDNO, consider only the valence electrons and neglect the differential overlaps for AOs on the same or different atoms. Among these different models, the expressions for Fock matrix $F$ may be different. The general semi-empirical Fock matrix is given by

$$F_{ij}(t) = T_{ij} + \sum_{kl} P_{kl}(t)(2V_{ij,kl} - V_{ik,lj}) \tag{14}$$

where $T$ is the time-independent one-electron integrals between AOs. The second and third terms on the RHS are the Coulumb and exchange contributions to the Fock matrix, respectively. In first-principles TDDFT, the exchange term is replaced by the exchange-correlation (XC) functional,

$$F_{ij}(t) = T_{ij} + \sum_{kl} P_{kl}(t)(V_{ij,kl} + V_{ij,kl}^{\mathrm{XC}}) \tag{15}$$

$V^{\mathrm{XC}}$ is the XC integral. In TDDFT, adiabatic approximation is commonly used where the static XC functional is evaluated with the time-dependent density and the memory is neglected. To improve the efficiency, an approximate DFT Hamiltonian, DFTB [42] is also implemented in LDM method. The TDDFTB Fock matrix is given by:

$$F_{ij}(t) = H_{ij}^0 + \frac{1}{2} S_{ij} \sum_a (\gamma_{ia} + \gamma_{ja}) \Delta q_a(t) \tag{16}$$

where $H^0$ is the time-independent Hamiltonian of a reference density. $\gamma$ gives a measure of the electron-electron interaction and decays asymptotically as $1/r$. For the on-site cases, the Hubbard-like parameter is taken from atomic DFT calculations and represents the chemical hardness of the respective element. $S$ is the overlap matrix and $\Delta q$ gives the Mulliken charge evaluated from the density matrix,

$$\Delta q_a(t) = \sum_{i \in a} \sum_j S_{ij} P_{ij}(t) \tag{17}$$

The update of Fock matrix is much more efficient in the DFTB method. It is shown from Eq. (16) that overlap matrix appears in the time-dependent part of the Fock matrix. In contrast to TDHF and TDDFT, the computational effort of constructing DFTB Fock matrix scales naturally linear by utilizing the sparsity of the overlap matrix and linear-scaling techniques introduced in Section 2 are not required.

Orthogonal basis is assumed in Eq. (7), the non-orthogonal basis employed in TDDFT and TDDFTB needs to be orthogonalized. Cholesky decomposition of the overlap matrix is used to orthogonize the Fock matrix and density

matrix, Alernatively, Eq. (12) represented in non-orthogonal basis can be solved directly [43].

$$\begin{aligned} i\hbar\delta\dot{P}^{(1)} &= \left(S^{-1}F^{(0)}\delta P^{(1)} - \delta P^{(1)}F^{(0)}S^{-1}\right) \\ &+\left(S^{-1}\delta F^{(1)}P^{(0)} - P^{(0)}\delta F^{(1)}S^{-1}\right) \\ &+\left(S^{-1}fP^{(0)} - P^{(0)}fS^{-1}\right) \end{aligned} \tag{18}$$

### 3.2 Applications

The LDM method has been applied to evaluate the optical spectra of different complex molecular systems. The optical spectrum can be obtained as the Fourier transform of the induced dipole moment which is computed from the induced density matrix $\delta P^{(1)}$. Liang *et al.* [44] applied the LDM method with PPP Hamiltonian to study the excited state properties of CNTs. Figure 1 shows the computational time versus the system size *N*. The number of carbon atoms in the CNTs ranges from 416 to 6656. A time interval of [−0.5 fs, −0.3 fs] with a time step of 0.01 fs is used. The cutoff lengths $l_0$ and $l_1$ are set to 15 Å and the CPU time is clearly proportional to the system size *N*.

Figure 2 plots the absorption spectra for $C_{320}H_{16}$, $C_{512}H_{16}$ and $C_{1024}H_{16}$ (8,0) CNTs simulated with the LDM method. FMM has been employed to construct the Fock matrix. The absorption spectra are similar in the high frequency region ($\omega > 1.5$ eV) with slight red shifts of the absorption peaks as the tube length increases and the spectral shape looks quite different in the low frequency region. Inspection of the induced density matrices $\delta P^{(1)}$ reveals that the small absorption peak at the very low energy region ($\omega < 0.3$ eV) corresponds to electronic excitations of electron-hole pairs between two ends of the nanotube, and disappears as the tube length increases.

Wang *et al.* [36] applied the LDM method with DFTB

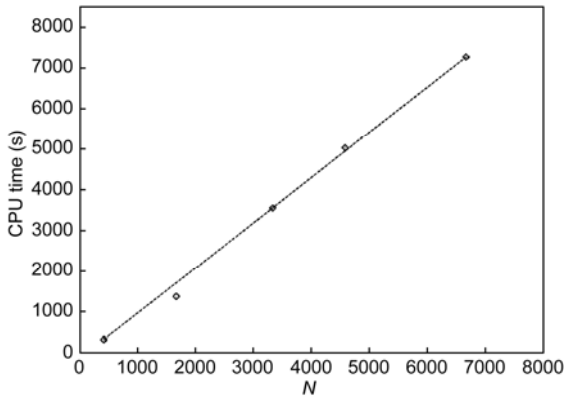


**Figure 1** CPU time for the excited-state calculation of 3-dimensional CNTs. The time interval is [−0.5 fs, −0.3 fs] with the time step of 0.01 fs. The cutoff lengths $l_0$ and $l_1$ are 15 Å. 26 atoms are included in the lowest level of the FMM box. (Figure adapted from Ref. [44]).

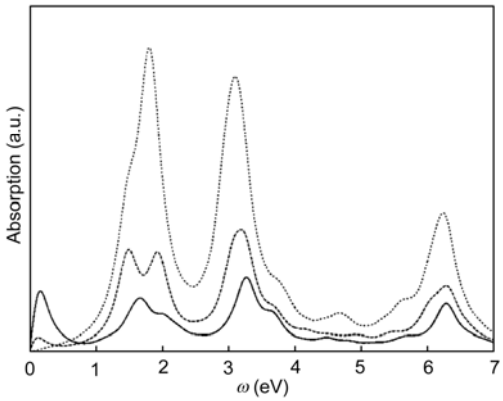


**Figure 2** Absorption spectrum of $C_{320}H_{16}$, $C_{512}H_{16}$ and $C_{1024}H_{16}$ calculated using the LDM method with PPP Hamiltonian. The cutoff lengths $l_0$ and $l_1$ are 36 Å . The dotted line stands for $C_{1024}H_{16}$, the dashed line for $C_{512}H_{16}$, and the solid line for $C_{320}H_{16}$. (Figure adapted from Ref. [44]).

Hamiltonian to calculate the optical response of 3-dimensional water clusters $[(H_2O)_{216}]_n$ ($n$ = 1, 2, 3, 4). Figure 3(a) shows the CPU time for a time propagation of 1 fs. The CPU time scales as $O(N^2)$ with the system size when no cutoff is applied, while it scales linearly using the LDM method with cutoff lengths $l_0$ and $l_1$ equal to 10 Å. The calculated absorption spectra of $(H_2O)_{864}$ are plotted in Figure 3(b), the black line represents the full TDDFTB calculation and red dots show the calculation with LDM method. It can be seen from Figure 3(b) that the error due to the cutoff of $\delta P^{(1)}$ is negligible. This is due to the fact that excitations of the system are mostly localized on a single water molecule and only influenced by nearby water molecules. A small cutoff length for $\delta P^{(1)}$ is thus adequate to obtain accurate absorption spectra.

## 4 TDKS with NOLMOs

Apart from the Liouville-von Neumann equation, there are also works devising methods to solve time-dependent Schrödinger equation with linear-scaling effort. Cui *et al.* [20] reformulated the TDKS equation in terms of NOLMOs $\varphi$ and obtained

$$i\hbar\frac{\partial}{\partial t}\varphi = H\varphi \tag{19}$$

Eq. (19) has the same form as the Schrödinger equation in canonical molecular orbital representation, except that the wave functions are replaced by the NOLMOs. The NOLMOs are the most localized representation of electron since the constraint of orthogonality is absent. In AO representation, NOLMOs can be expressed as

$$\varphi_\mu(t) = \sum_i^{\mathrm{AO}} c_{i\mu}\chi_i \tag{20}$$

and the density matrix can be obtained via Eq. (21)

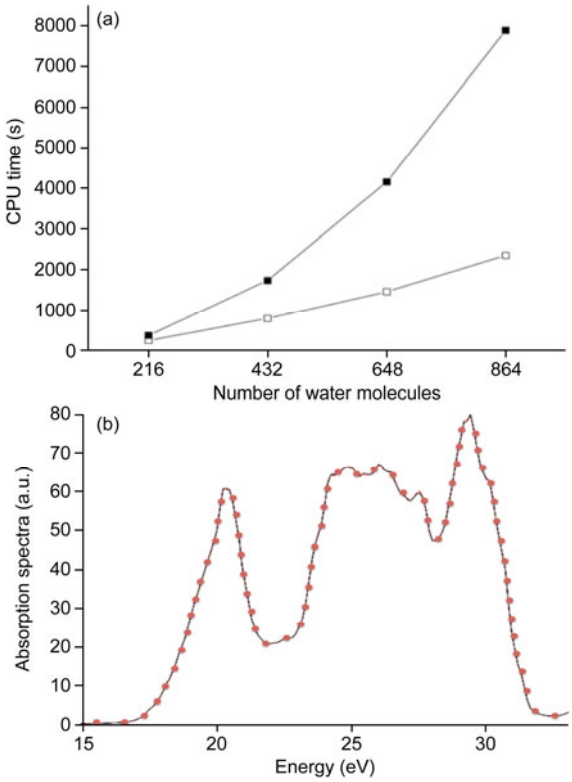


**Figure 3** (a) CPU time for water clusters with TDDFTB method in the time-domain with a propagation time of 1 fs (empty square: LDM method with 10 Å cutoff; filled square: full calculation). (b) Absorption spectra of $(H_2O)_{864}$ calculated with TDDFTB method in the time-domain (black line: full calculation; red line: LDM method with 10 Å cutoff).

$$P_{ij}(t) = \sum_{\mu\nu} c_{i\mu} S^{-1}_{\mu\nu} c^{*}_{j\nu} \tag{21}$$

Here, $c$ is the coefficient matrix. It should be noted that $S^{-1}$ is the inverse of overlap between NOLMOs. As NOLMOs are localized in space, each NOLMO spans only a finite set of AO in the system. Thus, the NOLMO sparsity is transferred to the coefficient matrix of molecular orbitals. This allows a linear-scaling computational effort for solving Eq. (19). One key point of the NOLMO approach is to maintain the sparisty of NOLMOs during the time propagation. As time proceeds, NOLMOs will become more delocalized and the sparsity of coefficient matrix is lost. The NOLMOs need to be reconstructed to ensure that the coefficient matrix remains localized. Therefore, the key of the O(N) calculation is that the coefficient matrix remains localized upon the repeated reconstruction of NOLMOs.

Cui *et al*. [20] applied the TDKS/NOLMO approach to simulate the absorption spectra of long chain saturated alkanes and conjugated alkenes with DFTB Hamiltonian. The same system has also been studied using LDM method with first-principles TDDFT [35]. Figure 4 plots the optical spectra of linear alkane, $C_{60}H_{122}$. Several cutoff lengths are employed to truncate the coefficient matrix. The interval time for reconstruction of NOLMOs is 1 au and the total propagation time is 100 au. It is clear that the error of TDKS/NOLMO approach decreases with the increase of the cutoff length.

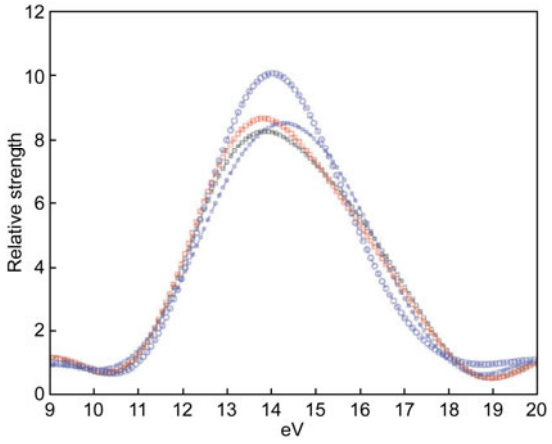


**Figure 4** The main peak of optical spectra of $C_{60}H_{122}$ with different cutoff lengths. Black diamonds: no cutoff; red diamonds: 10.6 Å; blue circles: 8.5 Å; blue diamonds: 7.4 Å. (Figure adapted from Ref. [20]).

## 5 Time integration

The EOMs of density matrix (Eq. (13)) or NOLMOs (Eq. (19)) are solved by numerical integration in time- domain. Common algorithms for time-domain integration include the Runge-Kutta method [45], the Exponential Midpoint method (EMM) [46] and the Magnus method [47]. A straightforward choice is the fourth order Runge-Kutta method. It has been implemented in both LDM method and the TDKS/NOLMOs approach. For the fourth order Runge-Kutta method, the ground state density matrix/NOLMOs are taken as the initial state. The density matrix/NOLMOs of the next time step are determined by the present value plus the weighted average of four increments evaluating at different times. This requires four evaluations of the Fock matrix for each time step. The largest possible time step is determined by the largest absolute eigenvalue of the Fock matrix [48] and normally a small time step has to be used to obtain accurate solution.

As an alternative, a high order method, the Chebyshev expansion method [49] is exploited in the LDM method. The solution for Eq. (13) is given by

$$\begin{aligned} \delta P^{(1)}(t) &= e^{-i\hat{L}t}\delta P^{(1)}(t=0) \\ &= \sum_{n=0}^{\infty}(2-\delta_{n0})J_n(t\Delta)P_n \end{aligned} \tag{22}$$

where $\hat{L}$ is the Liouville operator. The exponential term $e^{-i\hat{L}t}$ is expanded using Chebyshev expansion. Here $J_n(\alpha)$ is the Bessel function of the first kind. $P_n$ is given by

$$P_n = \frac{-2i}{\Delta}\hat{\boldsymbol{L}}P_{n-1} + P_{n-2},$$
$$P_1 = \frac{-i}{\Delta}\hat{\boldsymbol{L}}P_0, \quad (23)$$
$$P_0 = \delta P^{(1)}(t=0).$$

$\Delta$ is a positive number greater than largest eigenvalue of the Liouville operator for the expansion to converge. With $\delta P^{(1)}(t)$ obtained from Eq. (22), any $\delta P^{(1)}(t')$ with $t' < t$ can be determined through the above Chebyshev expansion with a minor additional effort. The Chebyshev expansion converges exponentially due to the exponential decay of the Bessel function $J_n(\alpha)$ when $n$ is larger than $\alpha$. It has been shown that Chebyshev expansion is much more efficient than fourth order Runge-Kutta method [50].

## 6 Conclusions

Linear-scaling quantum mechanical methods for excited states have been well developed, opening the way to study large complex molecular systems such as polymers, proteins, DNA, nano-materials and clusters which are previously intractable. In this article, we review the linear-scaling time-domain methods for excited states which are efficient, robust and can be readily implemented. Numerical algorithms are discussed and several applications are shown to demonstrate the effectiveness of these linear-scaling methods.

*We thank the Hong Kong Research Grant Council (HKU7009/09P, 7008/11P, and HKUST9/CRF/08), the Hong Kong University Grant Council (AoE/P-04/08) and the National Natural Science Foundation of China (21273186) for support.*

1 S. Goedecker. Linear scaling electronic structure methods. *Rev Mod Phys*, 1999, 71: 1085–1123
2 Bowler DR, Miyazaki T. O(N) methods in electronic structure calculations. *Rep Prog Phys*, 2012, 75: 036503
3 Schutz M, Hetzer G, Werner HJ. Low-order scaling local electron correlation methods. I. Linear scaling local MP2. *J Chem Phys*, 1999, 111: 5691–5705
4 Doser B, Lambrecht DS, Kussmann J, Ochsenfeld C. Linear-scaling atomic orbital-based second-order moller-plesset perturbation theory by rigorous integral screening criteria. *J Chem Phys*, 2009, 130: 064107
5 Schutz M, Werner HJ. Low-order scaling local electron correlation methods. IV. Linear scaling local coupled-cluster (lccsd). *J Chem Phys*, 2001, 114: 661–681
6 Flocke N, Bartlett RJ. A natural linear scaling coupled-cluster method. *J Chem Phys*, 2004, 121: 10935–10944
7 Ziolkowski M, Jansik B, Kjaergaard T, Jorgensen P. Linear scaling coupled cluster method with correlation energy based error control. *J Chem Phys*, 2010, 133: 014107
8 Chwee TS, Szilva AB, Lindh R, Carter EA. Linear scaling multireference singles and doubles configuration interaction. *J Chem Phys*, 2008, 128: 224106
9 Yokojima S, Chen GH. Time domain localized-density-matrix method. *Chem Phys Lett*, 1998, 292: 379–383
10 Yam CY, Zhang Q, Wang F, Chen G. Linear-scaling quantum mechanical methods for excited states. *Chem Soc Rev*, 2012, 41: 3821–3838
11 Chen GH, Yokojima S. Linear scaling calculation of excited-state properties of polyacetylene. *Phys Rev B*, 1999, 59: 7259–7262
12 Niklasson AMN, Challacombe M. Density matrix perturbation theory. *Phys Rev Lett*, 2004, 92: 193001
13 Weber V, Niklasson AMN, Challacombe M. Ab Initio linear scaling response theory: Electric polarizability by perturbed projection. *Phys Rev Lett*, 2004, 92: 193002
14 Xiang H, Liang W, Yang J, Hou J, Zhu Q. Spin-unrestricted linear-scaling electronic structure theory and its application to magnetic carbon-doped boron nitride nanotubes. *J Chem Phys*, 2005, 123, 124105
15 Xiang HJ, Yang J, Hou JG, Zhu Q. Linear-scaling density matrix perturbation treatment of electric fields in solids. *Phys Rev Lett*, 2006, 97: 266402
16 Kussmann J, Ochsenfeld C. A density matrix-based method for the linear-scaling calculation of dynamic second- and third-order properties at the hartree-fock and kohn-sham density functional theory levels. *J Chem Phys*, 2007, 127: 204103
17 Wu F, Liu W, Zhang Y, Li Z. Linear-scaling time-dependent density functional theory based on the idea of "from fragments to molecule". *J Chem Theory Comput*, 2011, 7: 3643–3660
18 Kohn W. Density functional and density matrix method scaling linearly with the number of atoms. *Phys Rev Lett*, 1996, 76: 3168–3171
19 Chen GH, Mukamel S. Nonlinear polarizabilities of donor-acceptor substituted conjugated polyenes. *J Phys Chem*, 1996: 100: 11080–11085
20 Cui G, Fang W, Yang W. Reformulating time-dependent density functional theory with non-orthogonal localized molecular orbitals. *Phys Chem Chem Phys*, 2010, 12: 416–421
21 Greengard L, Rokhlin V. A fast algorithm for particle simulations. *J Comput Phys*, 1987, 73: 325 – 348
22 Ding HQ, Karasawa N, Goddard III WA. Atomic level simulations on a million particles: The cell multipole method for coulomb and london nonbond interactions. *J Chem Phys*, 1992, 97: 4309–4315
23 White C, Johnson B, Gill P, Head-Gordon M. The continuous fast multipole method. *Chem Phys Lett*, 1994, 230: 8–16
24 Strain M, Scuseria G, Frisch M. Achieving linear scaling for the electronic quantum coulomb problem. *Science*, 1996, 271: 51–53
25 Gill P. Molecular integrals over gaussian basis functions. *Adv Quantum Chem*, 1994, 25: 141– 205
26 Shao Y, Head-Gordon M. An improved J matrix engine for density functional theory calculations. *Chem Phys Lett*, 2000, 323: 425–433
27 Neese F. An improvement of the resolution of the identity approximation for the formation of the Coulomb matrix. *J Comput Chem*, 2003, 24: 1740–1747
28 Sierka M, Hogekamp A, Ahlrichs R. Fast evaluation of the Coulomb potential for electron densities using multipole accelerated resolution of identity approximation. *J Chem Phys*, 2003, 118: 9136–9148
29 Becke A. A Multicenter numerical-integration scheme for polyatomic-molecules. *J Chem Phys*, 1988: 88: 2547–2553
30 Scuseria G. Linear scaling density functional calculations with Gaussian orbitals. *J Phys Chem A*, 1999: 103: 4782–4790
31 Burant JC, Scuseria GE, Frisch MJ. A linear-scaling method for Hartree-Fock exchange calculations of large molecules. *J Chem Phys*, 1996, 105: 8969–8972
32 Schwegler E, Challacombe M, Head-Gordon M. Linear scaling computation of the fock matrix. II. Rigorous bounds on exchange integrals and incremental fock build. *J Chem Phys*, 1997, 106, 9708–9717

33 Ochsenfeld C, White CA, Head-Gordon M. Linear and sublinear scaling formation of Hartree-Fock-Type exchange matrices. *J Chem Phys*, 1998, 109: 1663–1669

34 Yam CY, Yokojima S, Chen GH. Linear-scaling time-dependent density-functional theory. *Phys Rev B*, 2003, 68: 153105

35 Yam CY, Yokojima S, Chen GH. Localized-density-matrix implementation of time-dependent density-functional theory. *J Chem Phys*, 2003, 119: 8794–8803

36 Wang F, Yam CY, Chen G, Wang X, Fan K, Niehaus TA, Frauenheim T. Linear scaling time-dependent density-functional tight-binding method for absorption spectra of large systems. *Phys Rev B*, 2007, 76: 045114

37 Ng M, Zhao Y, Chen G. Low-lying excited states of light-harvesting system II in purple bacteria. *J Phys Chem B*, 2003, 107: 9589–9600

38 Liang W, Wang X, Yokojima S, Chen G. Electronic structures and optical properties of open and capped carbon nanotubes. *J Am Chem Soc*, 2000, 122: 11129–11137

39 Yokojima S, Zhou D, Chen G. Photoexcitations in poly(*p*-phenylenevinylene) aggregates. *Chem Phys Lett*, 2001, 333: 397–402

40 Niehaus TA. Approximate time-dependent density functional theory. *J Mol Struc-Theochem*, 2009, 914: 38–49

41 Saad Y. *Iterative Methods for Sparse Linear Systems.* 2nd Ed. Philadelphia: Society for Industrial and Applied Mathematics. 2003

42 Elstner M, Porezag D, Jungnickel G, Elsner J, Haugk M, Frauenheim T, Suhai S, Seifert G. Self-consistent-charge density-functional tight-binding method for simulations of complex materials properties. *Phys Rev B*, 1998, 58: 7260–7268

43 Liang WZ, Yokojima S, Chen GH. Generalized linear-scaling localized-density-matrix method. *J Chem Phys*, 1999, 110: 1844–1855

44 Liang W, Yokojima S, Zhou D, Chen G. Localized-density-matrix method and its application to carbon nanotubes. *J Phys Chem A*, 2000, 104: 2445–2453

45 Press W, Flannery B, Teukolsky S, Vetterling W. *Numerical Recipes In C*. New York: Cambridge University Press. 1988

46 Baer R, Neuhauser D. Real-time linear response for time-dependent density-functional theory. *J Chem Phys*, 2004, 121: 9803–9807

47 Magnus W. On the exponential solution of differential equations for a linear operator. *Pure Appl Math*, 1954, 7: 649

48 Wang F, Yam CY, Chen G. Time-dependent density-functional theory/localized density matrix method for dynamic hyperpolarizability. *J Chem Phys*, 2007, 126: 244102

49 Baer R. Accurate and efficient evolution of nonlinear Schrodinger equations. *Phys Rev A*, 2000, 62: 063810

50 Wang F, Yam CY, Chen G, Fan K. Density matrix based time-dependent density functional theory and the solution of its linear response in real time domain. *J Chem Phys*, 2007, 126: 134104